

## CHAPTER II

### THEORETICAL BACKGROUND AND LITERATURE REVIEW

#### 2.1 Background

Nowadays, environmental pollution due to the use of fossil fuels as well as their shortfall makes it necessary to find alternative energy sources that are environmentally friendly and renewable. Hydrogen is widely thought to be an ideal and efficient energy carrier of the future due to its high conversion efficiency, recyclability, and nonpolluting nature (Niu *et al.*, 2010). During the last decades, fuel cells have been recognized as an efficient and clean technology to produce energy for mobile applications (Horny *et al.*, 2004). Fuel cell vehicle based on PEMFCs can use hydrogen in an electrochemical cell to convert chemical energy directly into electricity for use with an electric motor (Gu *et al.*, 2003). The hydrogen required for the operation of PEMFCs vehicles may be stored either in high pressure tanks or generated on-board using a liquid hydrogen carrier such as methanol. Presently, direct storage and use of hydrogen on PEMFCs vehicles have certain limitations (Patel *et al.*, 2007a). Methanol is a primary candidate as a hydrogen carrier for on-board production of hydrogen for fuel cells, because it is a low cost fluid, virtually sulphur-free, safe to handle and easy to produce (Lenarda *et al.*, 2007). Methanol can be produced from natural gas, coal, other fossil fuels as well as renewable resources. H<sub>2</sub> production from methanol may involve various reactions (Gu *et al.*, 2003). So hydrogen production can be promising way for future alternative fuel that has a lot of advantages if you choose the suitable way for hydrogen production according to your applications.

#### 2.2 Hydrogen Production from Methanol (CH<sub>3</sub>OH)

Increasing global energy shortage and more stringent emission regulations have affected to improve the performance in the fuel cell. Hydrogen fed PEMFC is considered as a suitable system for automotive applications due to its environmental compatibility and higher energy conversion efficiency. The main problems faced

when using hydrogen as the fuel in a fuel cell vehicle are those related with storage, safety, and refueling. One solution to this difficulty is the on-board hydrogen generation from a suitable high-energy liquid fuel (Chang *et al.*, 2006). From different liquid fuels, methanol is considered to be a potential resource for hydrogen production due to its availability, high hydrogen-to-carbon ratio (4:1), no carbon-carbon bond (thus minimizing coke formation), conversion takes place at relatively low temperatures, high hydrogen content in the product stream (up to 75%), no sulfur presents in the fuel and current infrastructure of gasoline can be used for storage and distribution of methanol (Patel *et al.*, 2007b). In addition, it is low cost fuel, low boiling point, and high energy density liquid fuels. Moreover, as methanol can be produced from renewable sources, its reforming does not contribute to a net addition of CO<sub>2</sub> to the atmosphere (Perez-Hernandez *et al.*, 2008). The hydrogen production from methanol is also attractive due to the relatively low selectivity to by-products such as carbon monoxide and methane compared to alkane or higher alcohol reforming. Hydrogen may be produced directly from methanol according to a number of different processes such as methanol decomposition (MD), water gas shift reaction (WGSR), steam reforming (SRM), partial oxidation (POM) or oxidative steam reforming (OSRM) (Chen and Lin, 2010). From the several advantages of methanol have attracted much attention for hydrogen production.

### 2.2.1 Steam Reforming of Methanol (SRM)

The production of hydrogen by steam reforming of methanol (SRM) is currently of great interest for the development of fuel cell powered devices, especially for mobile applications. The chemical reaction considered for describing the SRM process:



The steam reforming of methanol (SRM) is an endothermic reaction and produces the highest yield of hydrogen, about 75%. Under this condition, 3 mole of hydrogen are produced for 1 mole of fuel, while maintaining a low selectivity of CO of less than 1% (Huang *et al.*, 2009). The reaction occurs at relatively low

temperature in the range of 200–300 °C. As a consequence, only a relative small amount of CO (<2%) is formed, which can be eliminated by preferential oxidation reaction. The endothermicity of the reaction, however, requires permanent external heating of the reformer which makes short start-up times and fast transient behavior difficult to achieve (Horny *et al.*, 2004).

This reaction produces a considerable amount of CO as a by-product. For the application of PEMFCs, even traces of CO (>20 ppm) in the reformed gas deteriorate a Pt electrode and the cell performance is lowered dramatically (Velu *et al.*, 2000). However, the development of productive and compact methanol processor demands to solve several challenges originating from the peculiarities of both the SRM, and the PEMFCs. A considerable amount (>100 ppm) of CO, which is a poison for Pt electrode in PEMFCs, is known to be produced during SRM, and a CO clean-up step of hydrogen prior to the fuelcell is required (Yaseneva *et al.*, 2008).

The steam reforming of methanol can also lead to the formation of toxic and undesirable products which limit the H<sub>2</sub> production, such as formic acid (HCOOH), formaldehyde (CH<sub>2</sub>O), and dimethyl ether (CH<sub>3</sub>OCH<sub>3</sub>) (Houteit *et al.*, 2006). Not only CO is usually found as by-product stream but also methane, depending upon the type of catalyst and the operating conditions. The formation of methane consumes hydrogen production from methanol and steam, resulting in suppressing the production of hydrogen gas, as shown in Equation 2.2.

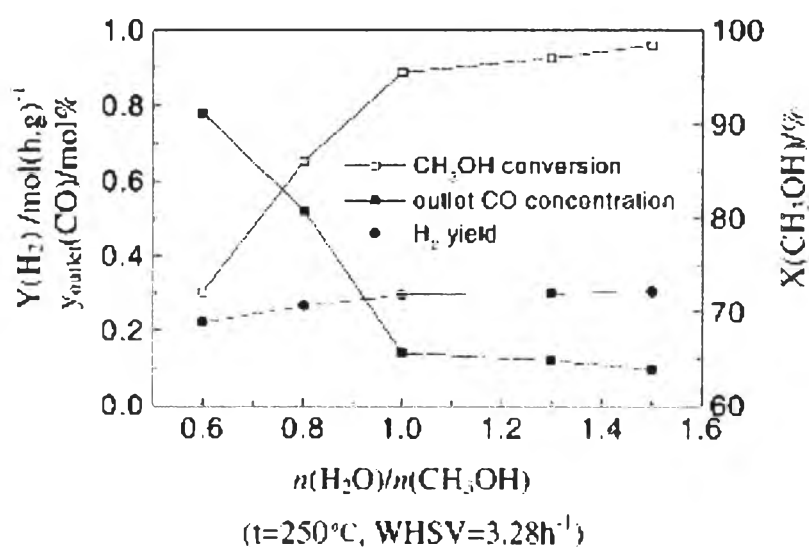


Both CO formation and CH<sub>4</sub> formation in SRM reaction can produce carbon formation. H<sub>2</sub> production operation concerns with regard to carbon formation. Carbon formation can build rapidly and shut down the process, thus it is important to keep it under control. There are two major pathways for carbon formation:



### 2.2.1.1 Experimental Condition

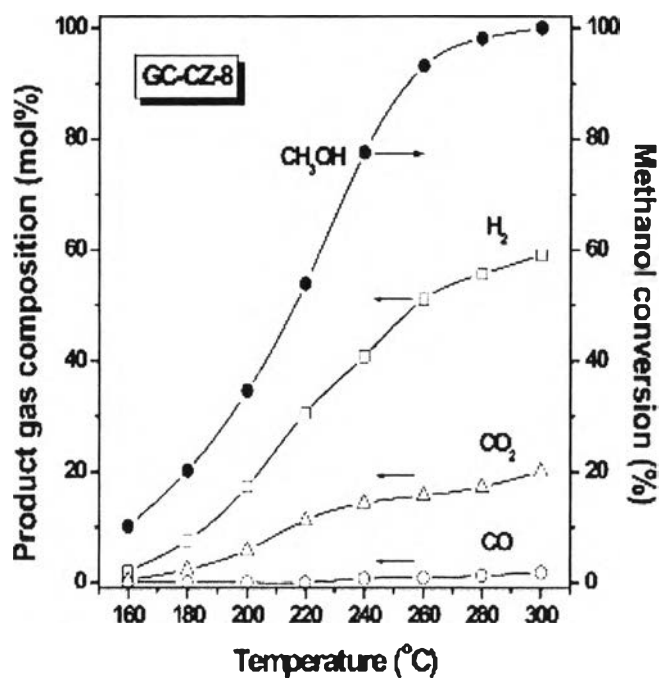
The effect of  $\text{H}_2\text{O}/\text{CH}_3\text{OH}$  molar ratio on the catalytic performance during the steam reforming of methanol reaction at  $250\text{ }^\circ\text{C}$  is shown in Figure 2.1. The methanol conversion increased with increasing the  $\text{H}_2\text{O}/\text{CH}_3\text{OH}$  molar ratio below 1.0, while the increase slows down beyond the ratio of 1.0.



**Figure 2.1** Effect of  $\text{H}_2\text{O}/\text{CH}_3\text{OH}$  molar ratio in methanol steam reforming reaction (Zhang and Shi, 2003).

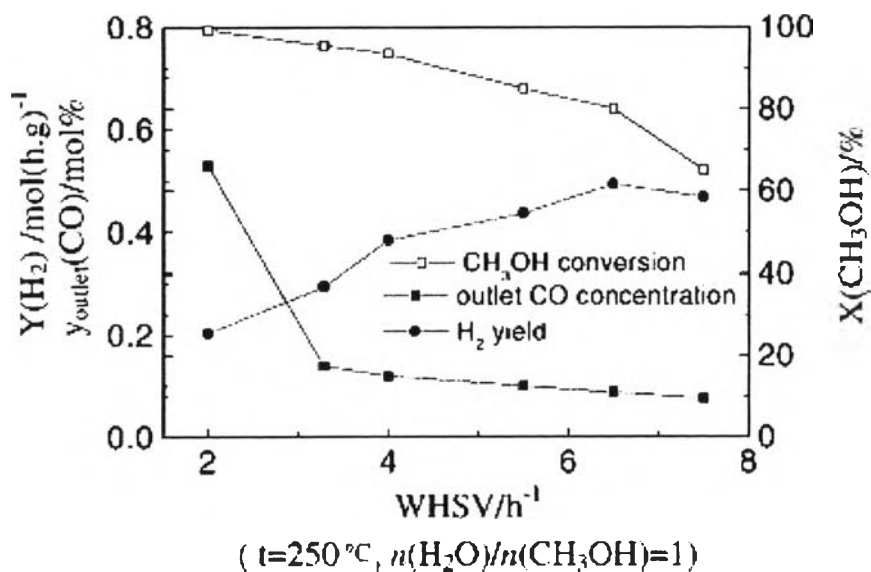
While hydrogen yield increases slowly with increasing  $\text{H}_2\text{O}/\text{CH}_3\text{OH}$  molar ratio. An outlet outlet CO concentration decreases to about 0.1 mol% with increasing the  $\text{H}_2\text{O}/\text{CH}_3\text{OH}$  molar ratio up to 1.5. The results showed that higher  $\text{H}_2\text{O}/\text{CH}_3\text{OH}$  molar ratio was favorable for reducing the outlet CO concentration due to the enhancement of WGS reaction.

The effect of the temperature on the methanol conversion and the molar composition with respect to carbon dioxide, hydrogen, and carbon monoxide on the catalytic activity was also investigated. Figure 2.2. shows that methanol conversion exhibits a typical S-shaped temperature dependence. The temperature at which complete conversion is achieved can be significantly lowered by decreasing the space velocity.



**Figure 2.2** Effect of reaction temperature on catalytic activity (Wang *et al.*, 2003).

The effect of methanol space velocity on the catalytic activity was also investigated. Figure 2.3 shows the effect of methanol space velocity (WHSV) on the catalytic performance of CeO<sub>2</sub> promoted catalysts. Methanol conversion and the outlet CO concentration decrease with increasing methanol space velocity, and hydrogen yield has a maximum in the experiment conditions. On the other hand, methanol space velocity does not affect the selectivity of H<sub>2</sub>, which remains around 99.9% throughout the experiment.



**Figure 2.3** Effect of methanol space velocity on the catalytic activity (Zhang *et al.*, 2003).

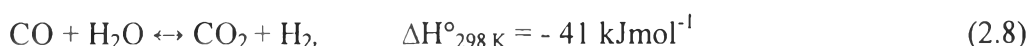
#### 2.2.1.2 Mechanism and Kinetics of Methanol Steam Reforming

There are limited kinetic studies and reaction mechanisms data available for the SRM process. The individual reactions to be included in the kinetic model of the SRM process are still under debate. Initially, SRM was supposed to proceed by the formation of CO and H<sub>2</sub> (DCM), followed by the WGS reaction. The formation of CO<sub>2</sub> by the direct reaction of methanol and steam has also been proposed (Mastalir *et al.*, 2005). Therefore, its concentration in the product stream must be equal to or greater than the concentration of CO at the WGSR equilibrium. The elementary surface reaction mechanisms and derived the Langmuir–Hinshelwood expression. They suggested that CO was formed via decomposition of methyl formate (Equations 2.5–2.7).



The kinetic expression from this predicts the rates of methanol conversion and carbon dioxide formation. They neglect the CO formation that cannot

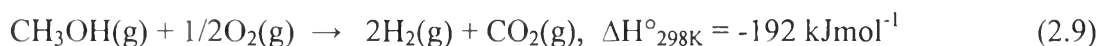
be neglected as even very low CO concentration can poison the Pt anode of PEM fuel cell. Development of a LH rate expression considering SRM, DCM, and WGS reactions with dual site mechanism. It can be seen that in all the reaction mechanisms the route of CO formation is different. The study CO formation mechanism through DRIFT analysis and confirmed that the CO formation over CuO/ZnO/ZrO<sub>2</sub>/Al<sub>2</sub>O<sub>3</sub> catalyst for SRM occurs via (RWGS) reaction (Equation 2.8). After that, many researchers have also proposed the CO formation via RWGS that uses the products of the reforming reaction i.e. H<sub>2</sub> and CO<sub>2</sub>.



The reaction rate of methanol and water consumption is depending only on the concentration of methanol but no depending on water concentration. Furthermore, the reaction rate of CO formation is a zero-order rate, which means that the formation of CO is not affected by the concentration of methanol or the concentration of water (Amphlett *et al.*, 1994).

### 2.2.2 Partial Oxidation of Methanol (POM)

The partial oxidation of methanol is an exothermic reaction with a rapid start-up but the formation of hot spots may result in the sintering of the catalysts (Huang *et al.*, 2009). Partial oxidation of methanol is an attractive on-site source of H<sub>2</sub> for fuel cells. This is an exothermic reaction according to equation:



Partial oxidation of methanol (POM) offers a potential process of producing hydrogen through an exothermic reaction. In the previous studies, it was reported that supported Cu, Pd, Pt and Au catalysts are active for hydrogen generation from methanol by POM (Chang *et al.*, 2008). The hydrogen content in the product gas is low (40% with air operation). Moreover, the high exothermicity of the reaction drastically lowers the efficiency of the process since waste heat is generated and temperature control of the reactor may be complicated (Horny *et al.*, 2004).

A number of other reactions can take place at the same time. These are mainly total methanol oxidation (Equation 2.10), methanol decomposition (Equation 2.11), steam reforming (Equation 2.12), water-gas shift (Equation 2.13), methanation (Equation 2.14), and CO (Equation 2.15) and H<sub>2</sub> (Equation 2.16) oxidation: (Perez–Hernandez *et al.*, 2007)

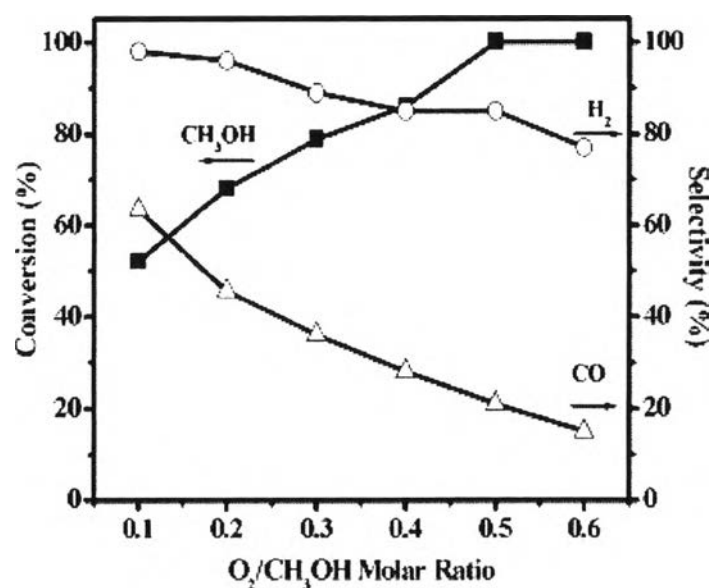


The POM reaction to produce H<sub>2</sub> has many advantages exist over the SRM since using oxygen (or air) instead of steam as the oxidant offers an exothermic reaction, more favorable thermodynamically, that resulting in more energy efficient. It can lessen the time needed for the apparatus to reach the working temperature from cold start-up and work under thermo-balanced conditions. In addition, it has been reported that the reaction rate of partial oxidation over copper catalysts is higher than the steam reforming reaction. However, the POM process is highly exothermic, heat must be removed from the reactor, and it could be difficult to control the temperature of the system (Wang *et al.*, 2003).



### 2.2.2.1 Catalytic Activity

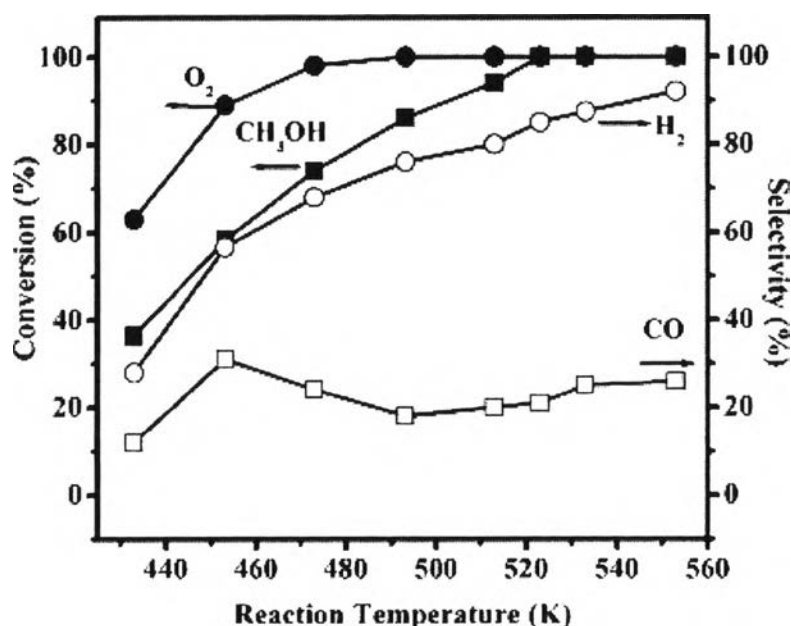
The effect of  $O_2/CH_3OH$  molar ratio on the activity of Au–Ru/ $Fe_2O_3$  catalysts at 250 °C is shown in Figure 2.4. With an increase in  $O_2/CH_3OH$  molar ratio, the amount of oxygen increases, methanol conversion increases from 52.0 to 100%. On the other hand, the hydrogen selectivity decreases with consequent increase in the selectivity of water. This could be due to fast oxidation of hydrogen formed in the reaction (Equation 2.16). CO selectivity was decreased with an increase in  $O_2/CH_3OH$  molar ratio due to the more availability of oxygen. Since a  $O_2/CH_3OH$  molar ratio of 0.5 showed higher hydrogen selectivity with complete conversion of methanol.



**Figure 2.4** Effect of  $O_2/CH_3OH$  molar ratio on methanol conversion, hydrogen selectivity and CO selectivity for partial oxidation of methanol over Au–Ru/ $Fe_2O_3$  catalysts (calcination temperature, 400 °C; reaction temperature, 250 °C; reaction time, 10 min) (Chang *et al.*, 2008).

The effect of reaction temperature on methanol conversion, oxygen conversion, hydrogen selectivity and CO selectivity for POM reaction over Au–Ru/ $Fe_2O_3$  catalyst was investigated. The study was undertaken in the temperature range between 160 and 280 °C. It can be observed that methanol conversion

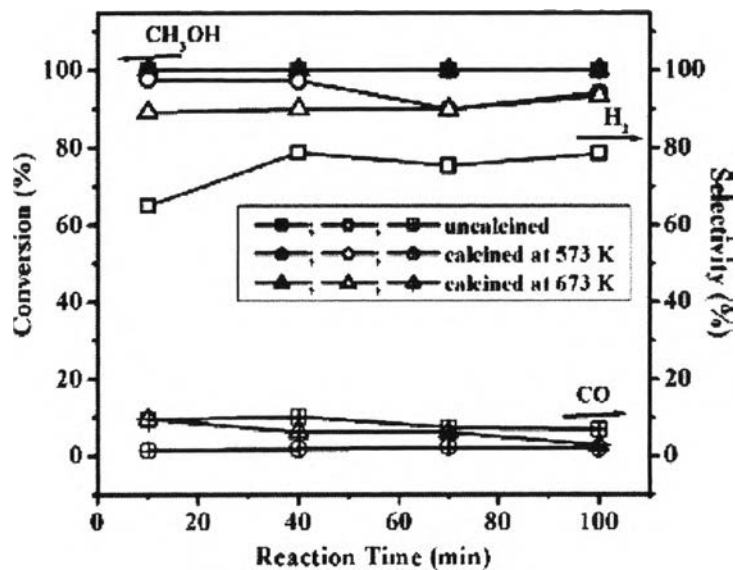
increased with increasing the reaction temperature and reached 100% at 250 °C. Oxygen conversion increases with increasing the reaction temperature. Complete consumption of oxygen was observed at 220 °C. Hydrogen selectivity reached 100% at 250 °C while the CO selectivity decreases with increasing the reaction temperature till 250 °C.



**Figure 2.5** Effect of reaction temperature on methanol conversion, oxygen conversion, hydrogen selectivity and CO selectivity for partial oxidation of methanol over Au–Ru/Fe<sub>2</sub>O<sub>3</sub> catalysts (calcination temperature, 400 °C; O<sub>2</sub>/CH<sub>3</sub>OH molar ratio, 0.5; reaction time, 10 min) (Chang *et al.*, 2008).

#### 2.2.2.2 Experimental Condition

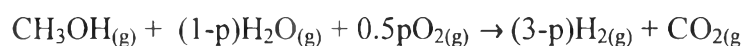
The effect of calcination temperature on methanol conversion, hydrogen selectivity, and carbon monoxide selectivity for partial oxidation of methanol at 250 °C was studied. Methanol conversion is 100% and independent of reaction time. But it is clear that calcination condition significantly influence the performance of the catalyst towards hydrogen formation. The hydrogen selectivity over Au/CuO/ZnO catalysts decreases in the following order: calcined at 300 °C > calcined at 400 °C > uncalcined. Thus, the optimum calcinations temperature is 300 °C.



**Figure 2.6** Effect of calcination temperature on methanol conversion, hydrogen selectivity and carbon monoxide selectivity for partial oxidation of methanol over Au/CuO/ZnO catalysts (reaction temperature, 250 °C) (Yang *et al.*, 2007).

### 2.2.3 Oxidative Steam Reforming of Methanol (OSRM)

The Oxidative steam reforming of methanol (OSRM) or autothermal reforming of methanol (ATRM) is a combination of steam reforming and partial oxidation. This process uses the energy produced from partial oxidation to supply the endothermic, steam-reforming reaction, and thus can be run adiabatically. This eliminates the need to transfer heat across a heat-conducting boundary and allows the reaction to proceed at much higher rates in a smaller reactor volume. Oxidative steam reforming of methanol (OSRM) has not been extensively studied, but initial results indicate low carbon monoxide yield and high hydrogen concentration in the products (Perez-Hernandez *et al.*, 2007). The equation can be written as:



$$\Delta H^\circ_{298\text{K}} = -241.8p + 49.5 \text{ kJmol}^{-1} \quad (2.17)$$

The overall heat of reaction depends upon the value of  $p$ , which directly influences the thermal properties of the OSRM system as well as hydrogen concentration (Patel *et al.*, 2007b).

Reactors for this process operate autothermally, i.e. does not require any external heating or cooling once heating reached the reaction temperature. The maximum obtainable hydrogen content in the product gas is 73% with oxygen in the feed 65% if air is used. For fast start-up or transient response the methanol/oxygen ratio can be varied as shown for the Hot-Spot reformer (Horny *et al.*, 2004). Oxidative steam reforming of methanol can be a promising way due to its energy saving, fast startup, and quick response of the overall reaction (Patel *et al.*, 2007b). Unfortunately, the OSRM process produces CO as a by-product in appreciable amounts which causes the poison for the Pt anodes of PEMFCs, and also suppresses the hydrogen's purity. To improve the activity of this reaction, the catalysts must be required in terms of high methanol conversion, high hydrogen selectivity, generating by the same time with minimizing of CO formation.

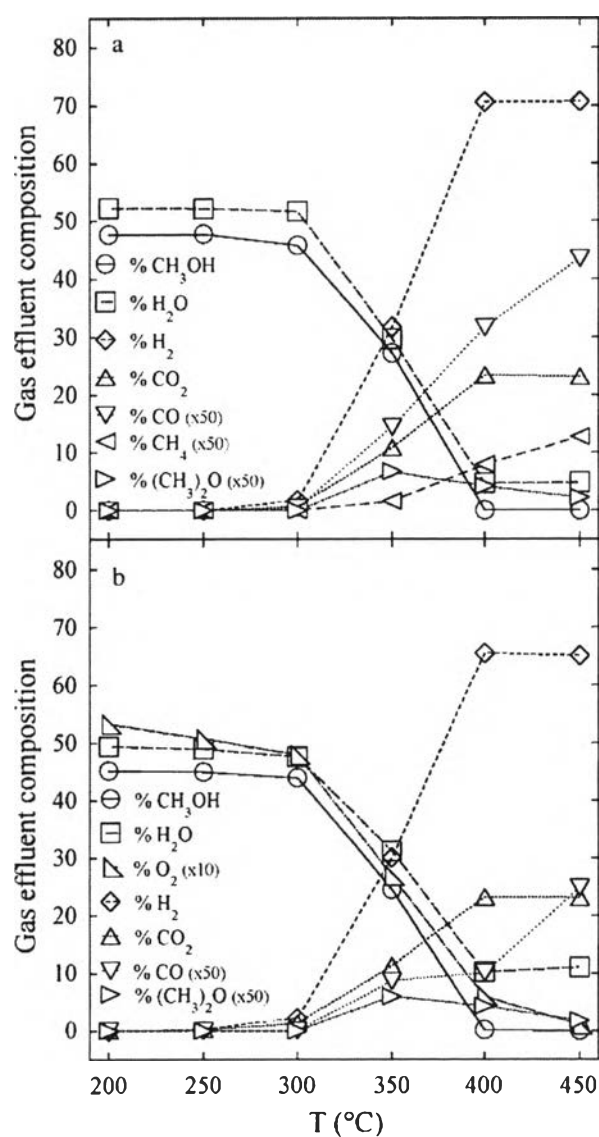
### 2.2.3.1 Experimental Condition

The effect of the temperature on the gas effluent composition in SRM and OSRM reactions over  $Zn_{10}Ti_{90}$  is shown in Figure 2.7. For both reactions, the main products are  $H_2$  and  $CO_2$ . The activity of the catalyst is negligible below 300 °C and above this temperature, it is active in methanol reforming (increasing of  $H_2$ ,  $CO_2$ , and decreasing of  $CH_3OH$  and  $H_2O$  (and  $O_2$  in OSRM)). The reactions are strongly influenced by the temperature and are complete at 400 °C. In both processes, CO and dimethylether ( $(CH_3)_2O$ ) are formed as by-products according to Equation 2.18. Methane is also produced in the SRM process. At temperature higher than 350 °C,  $(CH_3)_2O$  can react over titania surface in the presence of hydrogen, forming methane and water according to Equation 2.19. Thus, at temperature greater than 350 °C,  $(CH_3)_2O$  starts decreasing and simultaneously methane starts increasing in the SRM process.





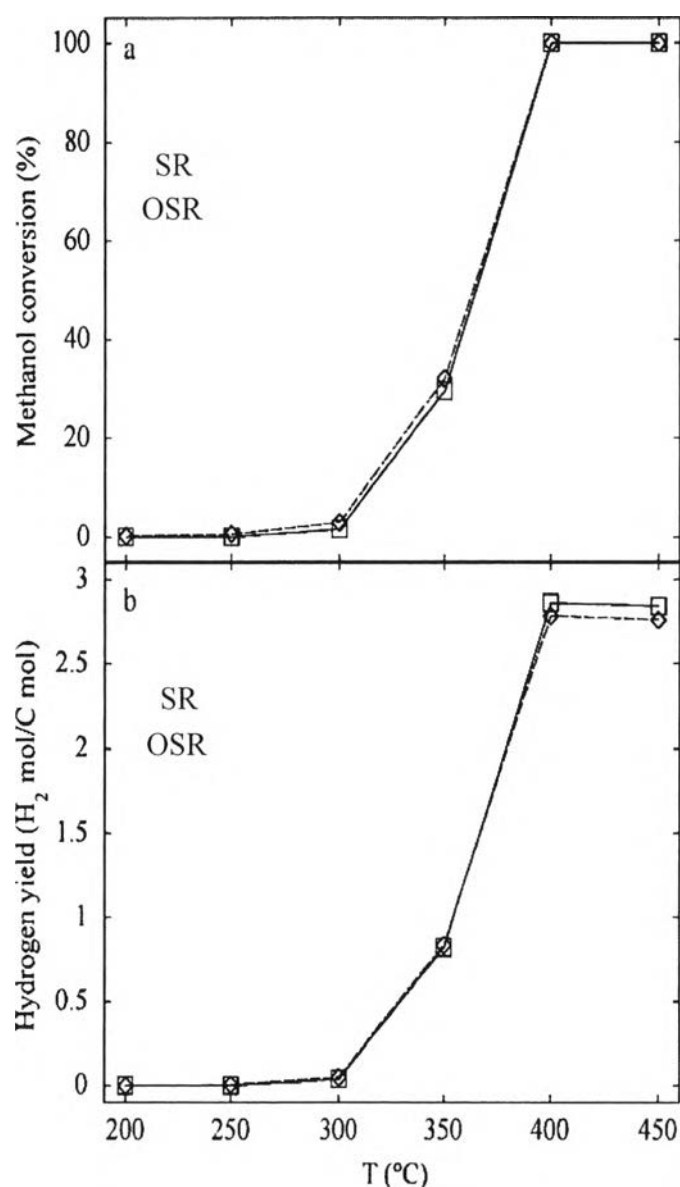
In the OSRM reaction, no methane is detected probably because the presence of  $\text{O}_2$  suppresses  $\text{CH}_4$  formation is shown in Equation 2.20.



**Figure 2.7** Effect of temperature on the gas effluent composition in the SRM (a) and OSRM (b) reactions over  $\text{Zn}_{10}\text{Ti}_{90}$  (Pinzari *et al.*, 2006).

In the OSRM process, the CO content is lower than in the SRM process, probably because of its oxidation to CO<sub>2</sub>.

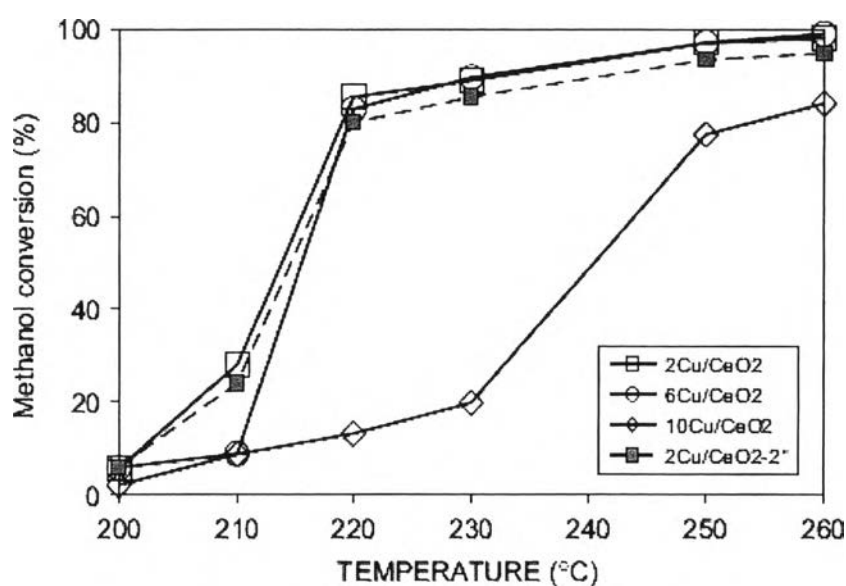
A comparison between the SRM and OSRM data is shown in Figure 2.8, the hydrogen production of SRM reaction starts at 300°C while the OSRM reaction starts at a lower temperature (250–300 °C), and shows slightly higher methanol conversion than SRM. At temperature of 400 °C, the hydrogen yield of OSRM (2.86) is higher than the hydrogen yield of SRM (2.78).



**Figure 2.8** Methanol conversion (a) and hydrogen yield (b) as a function of the temperature for Zn<sub>10</sub>Ti<sub>90</sub> (Pinzari *et al.*, 2006).

### 2.2.3.2 Catalytic Activity

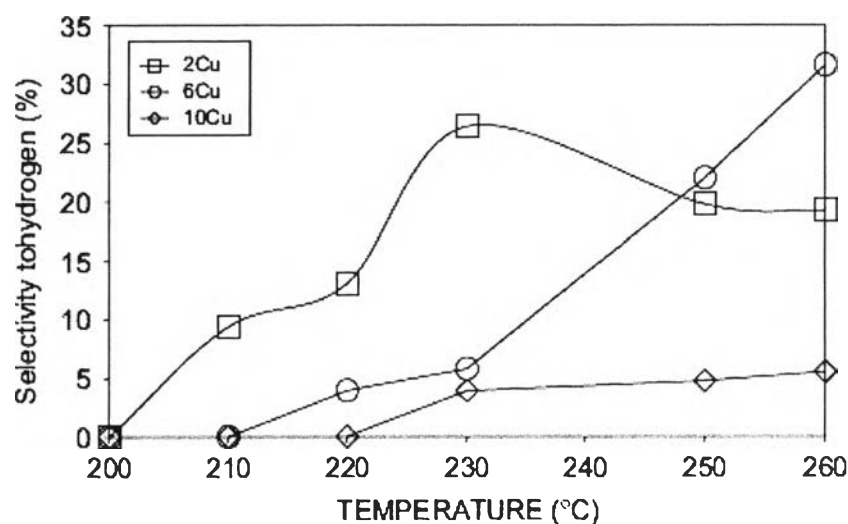
The catalytic performance of OSRM on Cu/CeO<sub>2</sub> catalysts is displayed in Figure 2.9. Methanol conversion reached almost 100% in the 2Cu and 6Cu catalysts, while in the 10Cu sample only 84% conversion was observed at the maximum reaction temperature. Sintering of highly dispersed copper on sample 10Cu during the OSRM reaction explains the low activity of this sample.



**Figure 2.9** Effect of temperature on the catalytic performance in the oxidative steam reforming of methanol over over  $n\text{Cu}/\text{CeO}_2$  catalysts. CH<sub>3</sub>OH partial pressure 30Torr, H<sub>2</sub>O partial pressure 4.6Torr and O<sub>2</sub> (5%)/He mixture (50 ml/min). GHVS = 30,000 h<sup>-1</sup>. Solid symbol corresponds to the second run in the OSRM reaction. Molar ratio O<sub>2</sub>/CH<sub>3</sub>OH = 0.83 and H<sub>2</sub>O/CH<sub>3</sub>OH = 0.15 (Perez-Hernandez *et al.*, 2007).

The effect of hydrogen selectivity on the catalytic performance during the steam reforming of methanol reaction on the Cu/CeO<sub>2</sub> catalysts. is shown in Figure 2.10. The 2Cu sample showed the best H<sub>2</sub> selectivity up to 230 °C, compared to other catalysts; after this temperature H<sub>2</sub> selectivity decreases in this sample and increases in the 6Cu catalyst. At the maximum reaction temperature in which almost all methanol is consumed, the final products were H<sub>2</sub>, H<sub>2</sub>O, and CO<sub>2</sub>. The H<sub>2</sub> depletion

observed on the 2Cu sample can be explained by the loss of active copper phase for the H<sub>2</sub> generation (Cu oxidation during the OSRM reaction).



**Figure 2.10** H<sub>2</sub> selectivity as a function of reaction temperature.  $\%S(H_2) = \frac{\text{mol}(H_2)}{(\text{mol}(H_2) + \text{mol}(CO_2))} * X_a$ ;  $\%S(CO_2) = \frac{\text{mol}(CO_2)}{(\text{mol}(H_2) + \text{mol}(CO_2))} * X_a$ ;  $X_a = \%$  methanol conversion (mol%) (Perez-Hernandez *et al.*, 2007).

### 2.3 Gold Catalyst

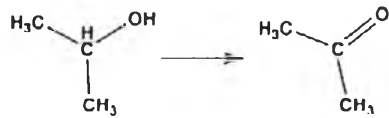
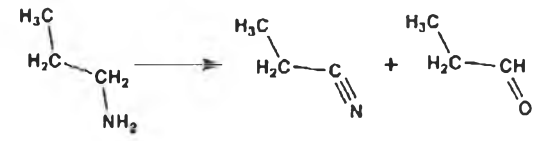
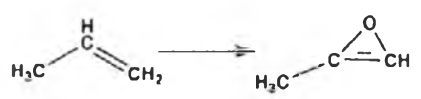
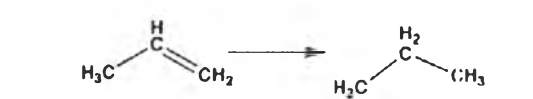

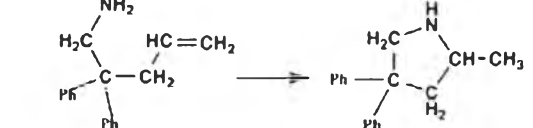
Gold has been regarded as a potentially useful catalyst system when it is highly dispersed on a suitable support for various industrial and environmental applications (Idakiev *et al.*, 2006). The demand for green catalysis—utilizing catalysts that reduce the environmental impact of chemical processes—requires selective, stable catalysts that function in a benign medium and can be easily recovered. It has been suggested that low-temperature reactions on noble metals, gold in particular may be part of the solution. The major factors for gold catalytic activity are including the size of gold nanoparticle, preparation method, pretreatment condition, and the nature of supports (Haruta., 1997). Gold catalysts show especially performance in the low-temperature oxidation of CO and the direct epoxidation of propene in the presence of hydrogen, where high selectivities of over 99% are achieved. Other important



reactions catalyzed by gold include water-gas shift, selective hydrogenations, hydrochlorinations, and selective oxidations of hydrocarbons and alcohols.

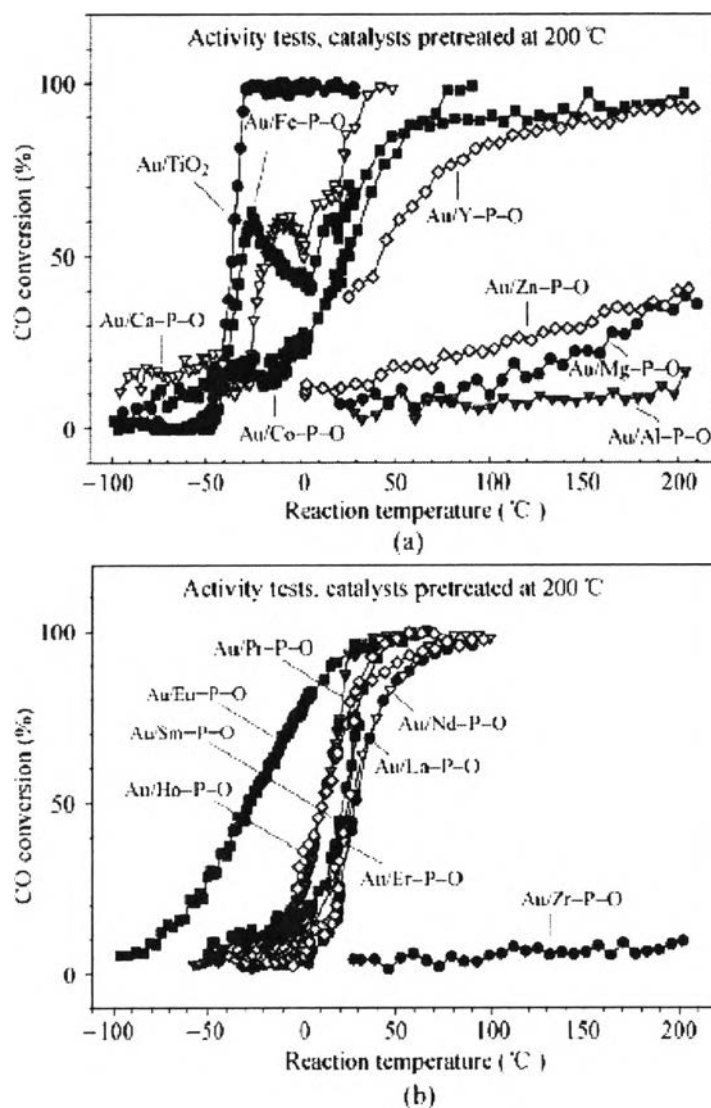
Deposition-precipitation (DP) is an effective method to deposit gold with high dispersion on MgO, TiO<sub>2</sub>, and Al<sub>2</sub>O<sub>3</sub>. This method is applicable to any forms of support including beads, honeycombs, and thin films. An important requirement is that the support materials should have high specific surface areas, preferably higher than 50 m<sup>2</sup>/g. Since gold hydroxide cannot be deposited at low pH, this method is useless for metal oxide having low points of zero charge (Haruta, 1997).

**Table 2.1** Gold facilitates a wide variety of reactions. The examples below are representative of this variety, and have been observed in solution and gas phase catalysis (Freyschlag and Madix, 2011)

 <p>Selective partial oxidation of alcohols</p>	 <p>Selective partial oxidation of amines</p>
 <p>Epoxidation</p>	 <p>Hydrogenation</p>
 <p>Esterification of alcohols</p>	 <p>Intra-molecular cyclization of amines and alkenes</p>

The gold particle size has extremely affect to activity of gold catalysts. Nanoparticles gold particles (5 nm) on mixed oxides have been shown to have superior activity for CO oxidation at low temperatures. In low temperature CO

oxidation, smaller Au nanoparticles deposited on metal oxides, such as  $\text{Mg}(\text{OH})_2$ ,  $\text{Al}_2\text{O}_3$ ,  $\text{TiO}_2$ , and  $\text{SiO}_2$ , show higher catalytic activity of CO oxidation. However, Haruta and Date' (2001) studied the deposited Au as nanoparticles on metal oxides by means of co-precipitation and deposition-precipitation techniques. It exhibited surprisingly high catalytic activity for CO oxidation. For systematically prepared an array of Au/M-P-O catalysts via deposition-precipitation are shown in Figure 2.11. Apart from Zr-P-O which was prepared by precipitation, the other M-P-O supports were purchased from a commercial supplier. Au/M-P-O (M= Ca, Fe, Co, Y, La, Pr, Nd, Sm, Eu, Ho, Er) showed high CO conversions when the reaction temperature was below 50 °C, whereas Au/M-P-O (M = Mg, Al, Zn, Zr) were not active, the activities of supported gold nanoparticles are not only related to the size of gold nanoparticles, but also influenced by the support and the preparation method. Considering the multiple functionalities of these catalysts (i.e., gold has its own catalytic function, and metal phosphates have acid-base properties).



**Figure 2.11** CO conversion curves of Au/TiO<sub>2</sub> and Au/M-P-O catalysts pretreated at 200 °C. Reproduced by permission of Springer from Ref (Ma and Dai, 2010).

The most striking phenomenon related to gold catalysis is the extreme dependence of the catalytic activity on the size of the Au particles, which also implies that sintering is very crucial for the long-term stability of the catalysts. The optimum size range is 2–5 nm; particles larger than ~20 nm show drastically reduced activities. This makes Au very different from classical catalysts based on transition metals such as Pt or Pd, which are also active as larger particles and even as macroscopic single crystals. In addition, it shows that the materials gap between Au single crystals on one side and real catalysts on the other plays an extraordinary role.

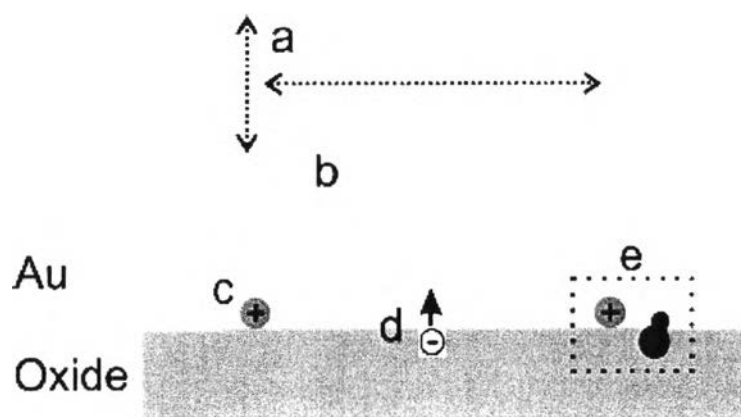
It is, therefore, essential to study a wide range of model systems with increasing complexity under comparable conditions to identify the structural, chemical or electronic features that are responsible for the catalytic activity (Gottfried and Erlangen-Nurnberg, 2003).

## 2.4 Supported Catalyst

Cerium oxide ( $\text{CeO}_2$ ) nanostructures are of considerable importance due to their optical properties: high thermal stability, electrical conductivity and diffusivity, and the ability to store and release oxygen, which have found wide applications such as high temperature ceramics, catalysts, fuel cells, silicon-on-insulator structures, barrier layers or capacitor devices. Ceria is a crucial component in the automobile three-way catalysts primarily for its role in oxygen storage, taking up oxygen under oxidising conditions and releasing it under reducing ones. Potential uses of  $\text{CeO}_2$  for the removal of soot from diesel engine exhaust, for the removal of organics from wastewaters, as an additive for combustion processes, and in fuel cell technology have been described (Yuan *et al.*, 2008).

Ceria is known to improve the stability of catalysts, increase the Au dispersion and the thermal stability of the catalysts, and even to reduce the CO concentration. Ceria exhibits accelerating action as support or promoter also in the reactions involving hydrogen such as hydrogenation of CO or methanol decomposition.  $\text{CuO/CeO}_2$  is effective for steam reforming of methanol (Oguchi *et al.*, 2005).

The morphology of the oxide support can also influence the state of the Au particles. For  $\text{Au/CeO}_2$ , cationic  $\text{Au}^{\delta+}$  species were found only in the case of nanocrystalline  $\text{CeO}_2$  (which also stabilizes the Au clusters) and not on  $\text{CeO}_2$  (111) films. Such effects can potentially limit the relevance of studies on planar model catalysts.

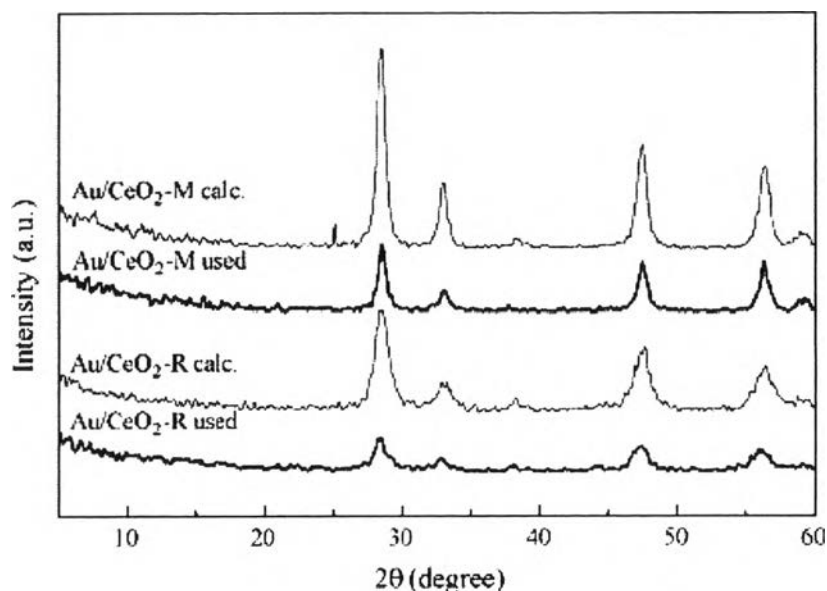


**Figure 2.12** Some of the models proposed for explaining the catalytic activity of Au/oxide catalysts: (a) Cluster size effects, (b) low-coordinated Au atoms, (c) cationic gold, (d) electron transfer from F centers of the support to the Au particle, (e) ensembles of Au<sup>0</sup>, Au<sup>+</sup>, and support-bound OH groups (Gottfried and Erlangen-Nurnberg, 2003).

To take advantage of the size effect of supports, Carrettin and co-workers used nanocrystalline CeO<sub>2</sub> (~4 nm, surface area of 180 m<sup>2</sup>/g) as a support for gold, and demonstrated that the activity of the resulting gold catalyst in CO oxidation was two orders of magnitude higher than that of a gold catalyst prepared by loading gold on a conventional CeO<sub>2</sub> support (surface area of 70 m<sup>2</sup>/g). They also found that nanocrystalline and mesostructured Y<sub>2</sub>O<sub>3</sub> could be used as supports for making active gold catalysts. In subsequent work, Carrettin and co-workers characterized Au/nanocrystalline CeO<sub>2</sub> and Au/nanocrystalline Y<sub>2</sub>O<sub>3</sub> in detail, and concluded that the existence of reactive peroxides at the gold-support interfaces was beneficial for enhancing the activity in CO oxidation (Carrettin *et al.*, 2005).

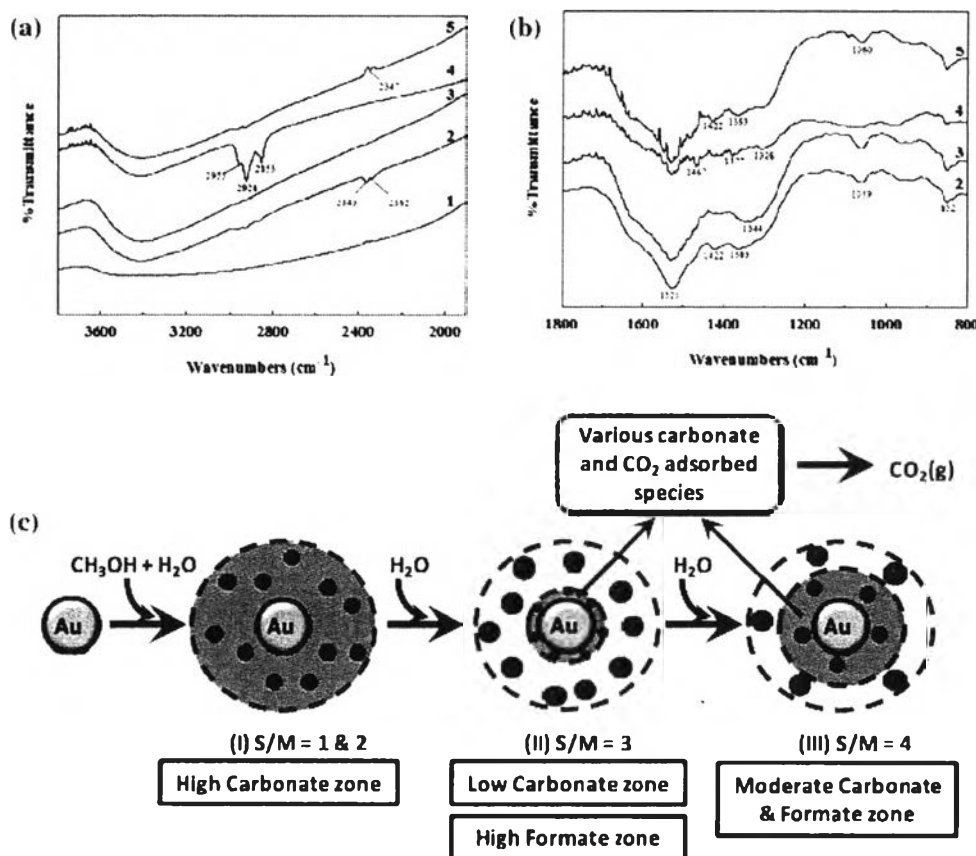
The XRD patterns of the Au/CeO<sub>2</sub> catalyst samples are shown in lists the enlarged patterns at 2θ range of 35–45° in order to show the diffraction lines of gold particles. Compared with the diffraction lines of pure mesoporous CeO<sub>2</sub> and nanorods shown in Figure 2.13, the Au/CeO<sub>2</sub>-R and Au/CeO<sub>2</sub>-M catalysts show weak diffraction lines of gold at 2θ = 38.28° and 44.48°, besides the fluorite phase

of CeO<sub>2</sub>. The average sizes of gold particles in Au/CeO<sub>2</sub>-R and Au/CeO<sub>2</sub>-M, determined from XRD line broadening of (1 1 1) by the Scherrer equation, are 11.1 and 6.3 nm, respectively.



**Figure 2.13** X-ray diffraction patterns of the gold-based catalysts calcined at 400 °C and after catalytic testing (used) (Yuan *et al.*, 2008).

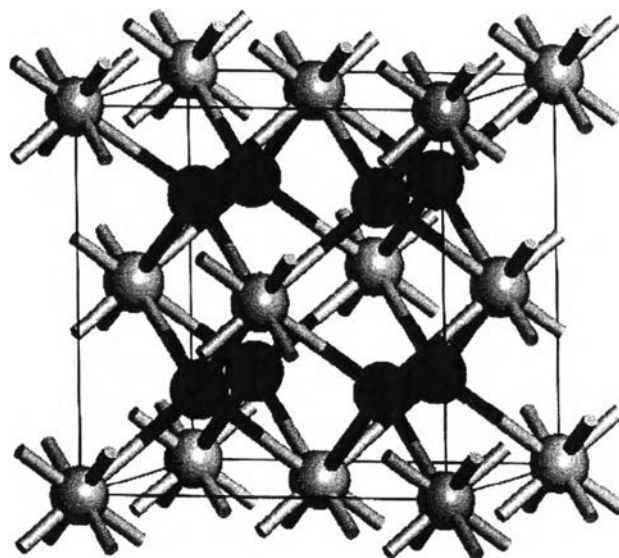
The FTIR spectra of the spent 1 wt% Au/CeO<sub>2</sub> catalysts with various H<sub>2</sub>O/CH<sub>3</sub>OH molar ratios is shown in Figure 2.14. A broad transmission in the OH region can be observed in the range of 3200–3600 cm<sup>-1</sup>, which follows the OH stretching mode of water molecules while the carbonate species on the surface were clearly detected in many positions, including unspecified carbonate species in the range of 800–1800 cm<sup>-1</sup> and 2500–3000 cm<sup>-1</sup>. Interestingly, the FTIR profile of the 3/1 H<sub>2</sub>O/CH<sub>3</sub>OH showed strong bands at 2853, and at 2924 and 2955 cm<sup>-1</sup>, relating to the formate species on Ce<sup>3+</sup> and Ce<sup>4+</sup>, which could also definitely block the active sites.



**Figure 2.14** FTIR spectra of 1 wt% Au/CeO<sub>2</sub> catalysts calcined at 400°C: (a – 2000–3600 cm<sup>-1</sup>; b – 800–1800 cm<sup>-1</sup>) (1) fresh catalyst; (2) after reaction at H<sub>2</sub>O/CH<sub>3</sub>OH molar ratio of 1/1; (3) after reaction at H<sub>2</sub>O/CH<sub>3</sub>OH molar ratio of 2/1; (4) after reaction at H<sub>2</sub>O/CH<sub>3</sub>OH molar ratio of 3/1; (5) after reaction at H<sub>2</sub>O/CH<sub>3</sub>OH molar ratio of 4/1 and (c) the schematic drawing of surface changing with various H<sub>2</sub>O/CH<sub>3</sub>OH (S/M) molar ratios (Pojanavaraphan *et al.*, 2012).

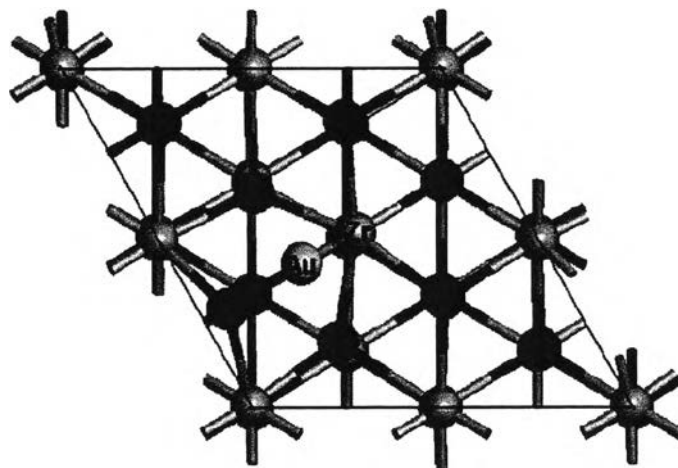
For another interesting support, Zirconia (ZrO<sub>2</sub>) can also participate in spillover effects, because the buildup of hydrogen that spills over from Cu I is possible on ZrO<sub>2</sub> as well. For the methanol synthesis reaction, ZrO<sub>2</sub> has the property of being able to adsorb CO<sub>2</sub>, where it can become hydrogenated. Likewise, for the steam reforming of methanol (SRM) reaction, ZrO<sub>2</sub> can readily adsorb methanol (Matter and Ozkan, 2005). The promoting effect of ZrO<sub>2</sub> has been attributed to the improvement in reducibility. ZrO<sub>2</sub> also reportedly increases the Cu dispersion and

prevents the sintering of Cu, due to its amorphous phase in catalyst.  $ZrO_2$  increases the amount of  $Cu^+$ , improving the activity and stability of the catalysts (Huang *et al.*, 2009). Oxide-supported metal play a pivotal role in a number of tecnologically important applications, including sensor, solid oxide fuel cells, and heterogeneous catalysts. Among the supports, Zirconia ( $ZrO_2$ ) is of specials interest owing to its ability at high temperature and other convenient mechanical and chemical properties that make it an attractive catalyst support for various reactions.  $Au/ZrO_2$  materials are of significant interest as catalyst for CO oxidation and for the selective hydrogenation of unsaturated compounds. The most active sites in a  $Au/ZrO_2$  catalyst for the selective hydrogenation reaction are isolated Au cations at the surface of zirconia, but in the general role of isolated gold species in these an other reactions is not clear.



**Figure 2.15** Crystal structure of cubic  $ZrO_2$ . Red and blue spheres correspond to oxygen and zirconium atoms, respectively (Grau-Crespo *et al.*, 2007).



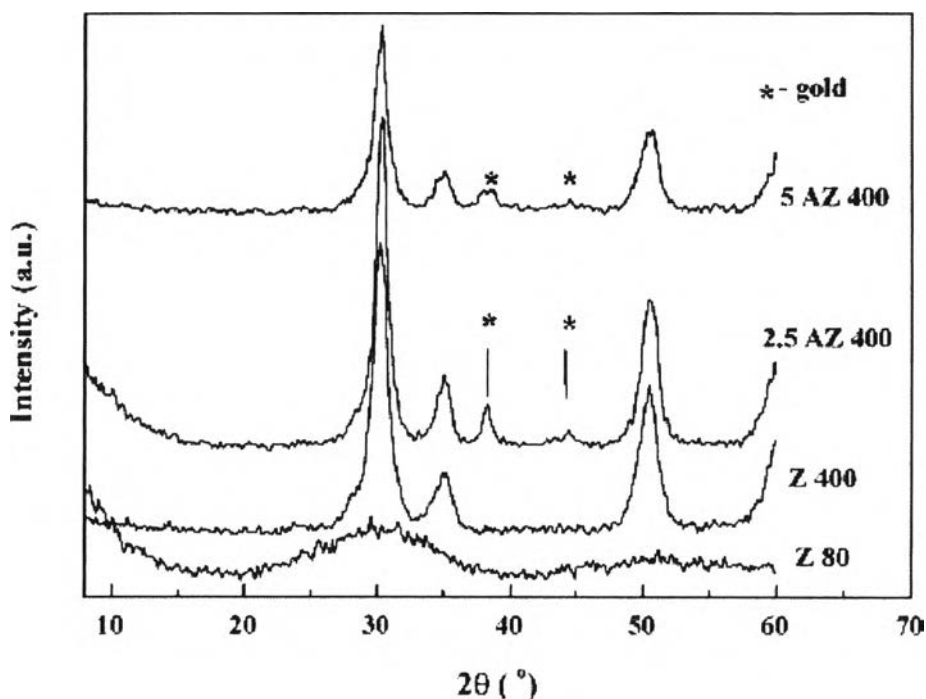


**Figure 2.16** Top view of the relaxed  $\text{ZrO}_2(111)$  surface with 0.25 ML of Au adsorbed at the most stable site (bridging between  $\text{O}_u$  and Zr). Upon adsorption, the  $\text{O}_u$  atom moves away from the Zr atom at the other side of the bridge. Similar relaxations take place upon the adsorption of Cu or Ag, but with different variations of the  $\text{O}_u$ -Zr distances (Grau-Crespo *et al.*, 2007).

The size effect of zirconia in Au/ $\text{ZrO}_2$  catalysts for CO oxidation was reported that nanocomposite Au/ $\text{ZrO}_2$  catalysts with comparably sized gold particles (4–5 nm) and  $\text{ZrO}_2$  nanoparticles (5–15 nm) were much more active in CO oxidation than those containing similarly sized gold particle but larger  $\text{ZrO}_2$  particles (40–200 nm). The reduction in the particle size of the support may not only create more contact between the metal and support, but also create more oxygen vacancies so that oxygen can be activated and migrate more easily. Similarly, Shen and co-workers prepared several gold catalysts with similar gold particle sizes on  $\text{ZrO}_2$  supports with different particle sizes, and found that the activity in the water-gas shift reaction decreased when the size of  $\text{ZrO}_2$  support particles was increased (Shen and Lee, 2001).

The X-ray diffraction patterns of the mesoporous zirconia as-prepared (Z 80) and calcined at 400 °C (Z 400), and gold-based catalysts calcined at 400 °C with different gold content (2.5 and 5 AZ 400) is shown in Figure 2.17. The X-ray diffractogram of the as-prepared mesoporous zirconia (Z 80) shows only a broad peak located in the  $2\theta$  range of 20 – 40°. The gold lines of catalyst 2.5 AZ 400 are observed more clearly than in the case of 5 AZ 400, while the zirconia diffraction

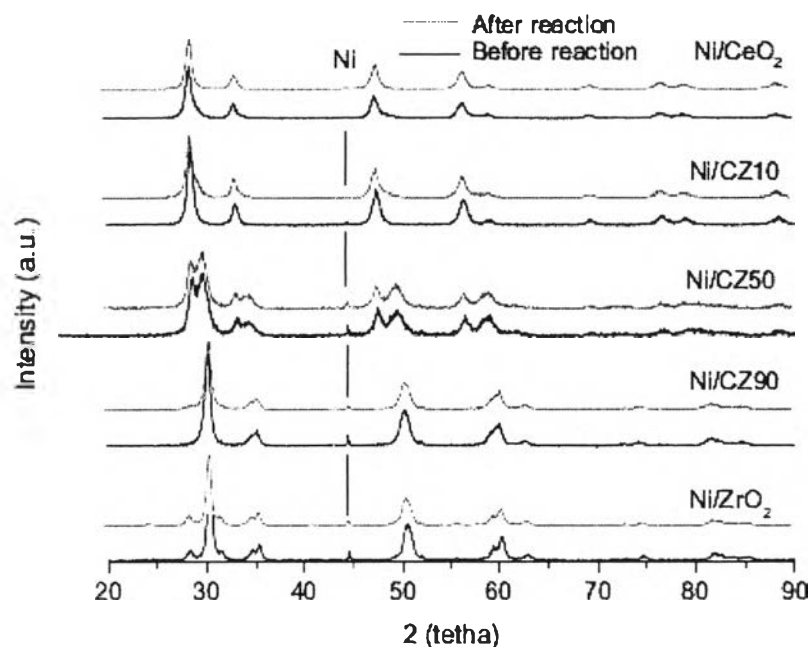
lines of 2.5 AZ 400 have a higher intensity than those of 5 AZ 400. The deposition of gold in higher content could restrain to a certain extent the crystallization of tetragonal  $\text{ZrO}_2$  phase and the enlargement of gold particle size, due to the possible interaction between  $\text{ZrO}_2$  and gold particle.



**Figure 2.17** X-ray diffraction patterns of the mesoporous zirconia as prepared (Z 80) and calcined at 400 °C (Z 400), and gold-based catalysts calcined at 400 °C with different gold content (2.5 and 5 AZ 400). \* Indicates the diffraction lines of gold (Idakiev *et al.*, 2006).

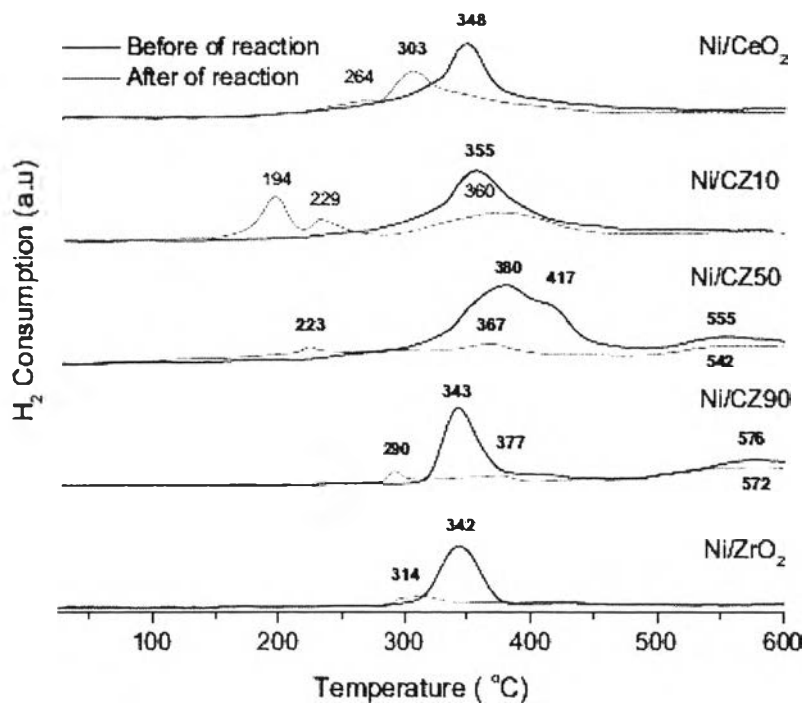
Perez-Hernandez *et al.*, 2011 studied the catalytic properties for hydrogen production by oxidative steam reforming of methanol over  $\text{Ni/CeO}_2\text{-ZrO}_2$  catalysts. XRD patterns of the  $\text{Ni/CeO}_2\text{-ZrO}_2$  catalysts are presented on Figure 2.18. For  $\text{Ni/ZrO}_2$  catalyst, the tetragonal and monoclinic phases of the zirconia was observed. The addition of  $\text{CeO}_2$  to  $\text{ZrO}_2$  on mixed oxides causes a reduction in the intensity and a broadening of the diffraction peaks. This finding was associated with the reduction of crystallinity, as well as a reduction in the particle size of the support. In addition, diffraction peak of the metallic Ni was observed in all samples; but the intensity of this peak was higher on the  $\text{Ni/ZrO}_2$ -rich samples than on the  $\text{Ni/CeO}_2$ -rich catalysts;

suggesting that  $\text{CeO}_2$  support promote the dispersion of Ni and make its crystallite size smaller.



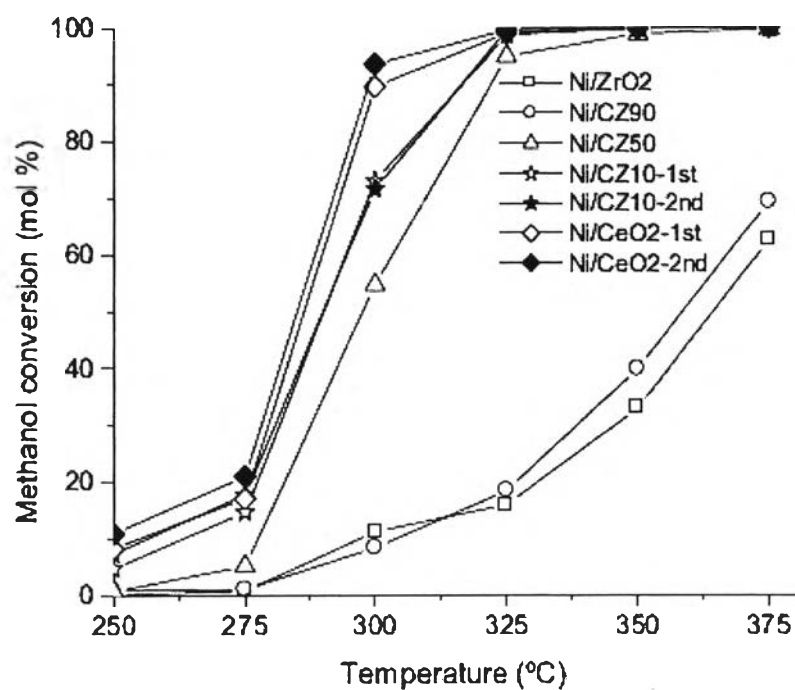
**Figure 2.18** XRD patterns of the Ni/CeO<sub>2</sub>-ZrO<sub>2</sub> catalysts before and after catalytic activity (Perez-Hernandez *et al.*, 2011).

The TPR profiles of the catalysts is shown in Figure 2.19, when increasing CeO<sub>2</sub> content to ZrO<sub>2</sub>, reduction temperature of the Ni-base catalysts supported on the mixed CeO<sub>2</sub>-ZrO<sub>2</sub> oxides shifted towards higher temperature until ZC-50 support. TPR profiles of the samples after OSRM reaction showed a shift of the reduction peaks at lower temperatures than on the fresh catalysts. This effect was associated with the redispersion of the active phase supported on CeO<sub>2</sub>-ZrO<sub>2</sub> oxides having highly dispersed species.



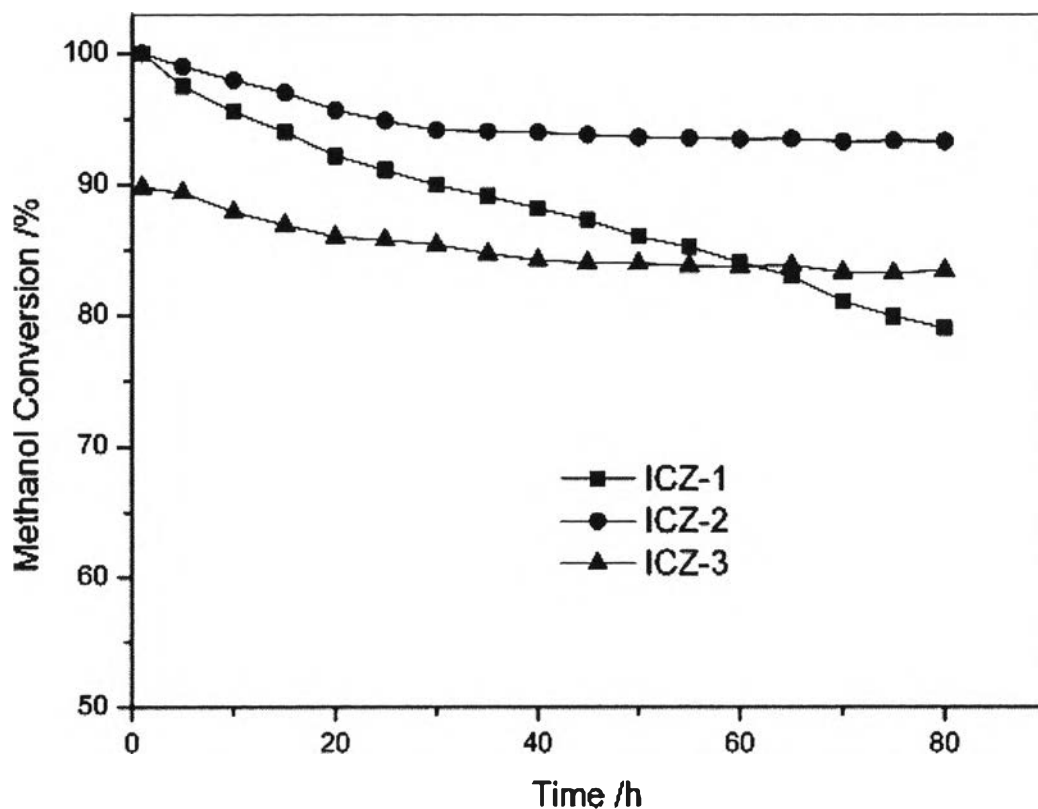
**Figure 2.19** Temperature-programmed reduction profiles of the fresh Ni/CeO<sub>2</sub>-ZrO<sub>2</sub> catalysts (solid line), samples after catalytic reaction (thin line) (Perez-Hernandez *et al.*, 2011).

The effect of the reaction temperature between 250 and 375 °C on the catalytic performance of Ni/CeO<sub>2</sub>-ZrO<sub>2</sub> catalysts during the OSRM reaction is illustrated in Figure 2.20. It can be seen that the conversion of methanol was high at the maximum reaction temperature. In addition, it was found that the activity strongly depends on the type of support and composition of support. Among the catalyst studied. The Ce-rich catalysts exhibit the highest methanol conversion, whereas nickel supported on Zr-rich supports gave the lowest activity.



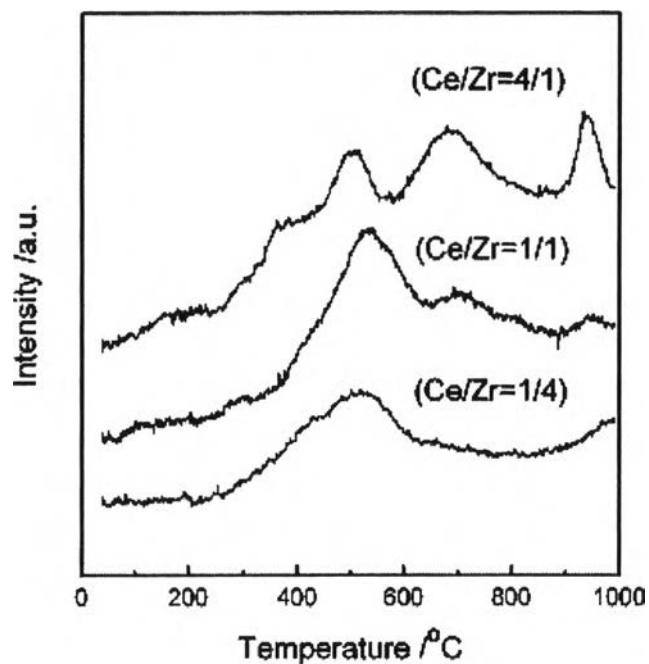
**Figure 2.20** Effect of temperature on the catalytic performance in the oxidative steam reforming of methanol over Ni/CeO<sub>2</sub>-ZrO<sub>2</sub> catalysts (Full symbol corresponds to the second cycle of reaction). Partial pressure of CH<sub>3</sub>OH, H<sub>2</sub>O and O<sub>2</sub> was 75, 12.75, and 25.2 Torr, respectively. GHVS 30,000 h<sup>-1</sup> (Perez-Hernandez *et al.*, 2011).

The effect of the CeO<sub>2</sub>/ZrO<sub>2</sub> ratio on the catalyst activity is illustrated in Figure 2.21. The results confirmed that CeO<sub>2</sub> was beneficial to catalyst activity, while the addition of a suitable level of ZrO<sub>2</sub> could enhance the long term stability. The optimum performance, both for activity and stability, was obtained for the sample with a 1:1 CeO<sub>2</sub>/ZrO<sub>2</sub> ratio.



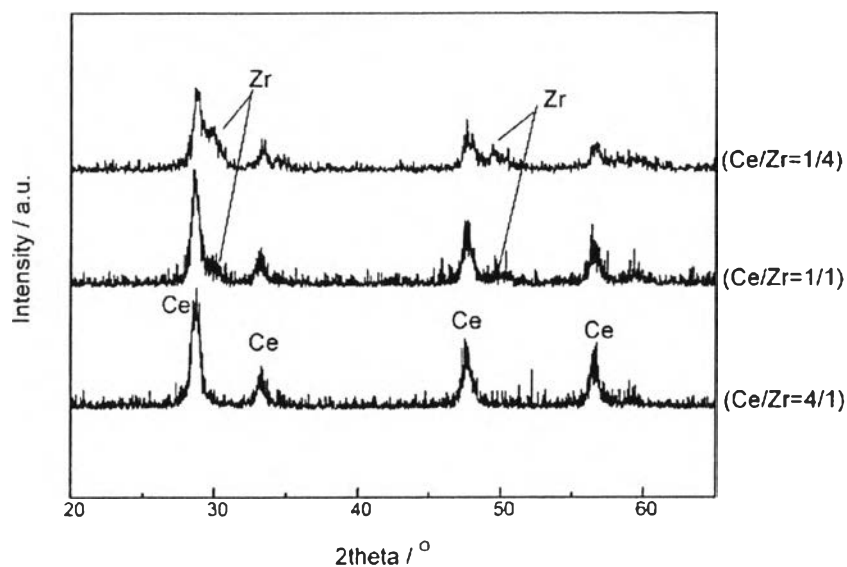
**Figure 2.21** Stability of catalysts with different Ce/Zr molar ratio supports. Reaction conditions: LHSV: 2.5 h<sup>-1</sup>, H<sub>2</sub>O/CH<sub>3</sub>OH: 1.5 mol mol<sup>-1</sup>, reaction temperature: 400 °C. Catalysts: 0.3 wt.-%Ir/CeO<sub>2</sub>-ZrO<sub>2</sub>, molar ratio of Ce/Zr: 4:1 (ICZ-1), 1:1(ICZ-2), and 1:4 (ICZ-3) (Zhang *et al.*, 2006).

The effect of different CeO<sub>2</sub>/ZrO<sub>2</sub> ratios could be further explained by the TPR profiles of the Ce<sub>x</sub>Zr<sub>1-x</sub>O<sub>2</sub> samples, shown in Figure 2.22. Ce-rich nanocrystallites dispersed well on the surface of the mixed oxides crystallites (947 °C). In conjunction with the increasing ZrO<sub>2</sub> content, the two lower temperature peaks merged into one peak at 527 °C, while the other high temperature peaks became weak. The sample had the low peak area at low temperature, indicating that its redox activity might be low.



**Figure 2.22** TPR profiles of  $\text{Ce}_x\text{Zr}_{1-x}\text{O}_2$  mixed oxides with different ratios (Zhang *et al.*, 2006).

Figure 2.23 shows the XRD patterns of  $\text{Ce}_x\text{Zr}_{1-x}\text{O}_2$  samples. Zr-rich sample has effect on the oxygen mobility through the  $\text{CeO}_2$  lattice, although the addition of  $\text{ZrO}_2$  could enhance the catalyst stability, the amount of  $\text{ZrO}_2$  in the mixed oxide should not be too high. It was found that a 1:1  $\text{CeO}_2/\text{ZrO}_2$  ratio seemed to be the best choice in terms of maintaining catalyst activity as well as stability.



**Figure 2.23** XRD patterns of  $\text{Ce}_x\text{Zr}_{1-x}\text{O}_2$  mixed oxides with different ratios (Zhang *et al.*, 2006).

All of these are the motivation in this work to study effect of composite support ( $\text{CeO}_2\text{-ZrO}_2$ ), Au content, steam to methanol molar ratio, oxygen to methanol molar ratio, and reaction temperature on the catalytic activity of  $\text{Au/CeO}_2\text{-ZrO}_2$  for the OSRM. In particular, the physical and electronic properties of a gold catalyst are greatly affected by using  $\text{CeO}_2\text{-ZrO}_2$  as a support.